Power Smoothing of Large Solar PV Plant Using Hybrid Energy Storage

Guishi Wang, *Student Member*, *IEEE*, Mihai Ciobotaru, *Member*, *IEEE*, and Vassilios G. Agelidis, *Senior Member*, *IEEE*

***Abstract*—This paper proposes a power smoothing strategy for a 1-MW grid-connected solar photovoltaic (PV) power plant. A hybrid energy storage system (HESS) composed of a vanadium redox battery and a supercapacitor bank is used to smooth the fluctuating output power of the PV plant. The power management of the HESS is purposely designed to reduce the required power rating of the SCB to only one-fifth of the VRB rating and to avoid the operation of the VRB at low power levels, thus increasing its overall efficiency. The PV plant including the HESS has been modeled using MATLAB/Simulink and PLECS software environment. The effectiveness of the proposed power control strategy is confirmed through extensive simulation results.**

***Index Terms*—Energy storage, flow batteries, photovoltaic (PV) systems, power control, power conversion, power smoothing, solar power generation, supercapacitors (SCs).**

I. Introduction

GRID-CONNECTED solar photovoltaic (PV) power plants are being installed at a fast pace globally. Currently, additional regulations and standards are expected to be imposed on large PV power plants, due to their potential adverse impacts on reliability and stability of the electricity network [1]–[3].

A possible solution for regulating the natural oscillating output power of a PV plant is to integrate an energy storage system (ESS) [1], [2], [4]–[7]. Battery ESSs (BESSs) are commonly used with renewable energy systems [4]–[7].

A BESS can use a wide range of technologies [1], [8], [9], such as lead-acid, Li-ion, sodium sulfur (NaS), vanadium redox (VRB), and many others. Nowadays, the lead-acid battery [1], [10] dominates the BESSs market, due to its relatively low manufacturing cost. However, the lifespan of such battery is typically less than 1000 full cycles and may be further shortened by deep discharge cycles. The Li-ion battery [1], [8], [9] has a very good performance in terms of efficiency. However, the limited availability of lithium and the special packaging lead to high costs for large-scale applications. The NaS battery [1], [8], [9] can be easily scaled to megawatt range but poses a potential safety risk due to its high operation temperature (300 °C–350 °C).

Manuscript received September 26, 2013; revised January 20, 2014; accepted January 28, 2014. Date of publication March 21, 2014; date of current version June 17, 2014.

The authors are with the Australian Energy Research Institute (AERI) & School of Electrical Engineering and Telecommunications, University of New South Wales (UNSW), Sydney, New South Wales 2052, Australia (e-mail: allen.wang@student.unsw.edu.au; mihai.ciobotaru@unsw.edu.au; vassilios.agelidis@unsw.edu.au).

Color versions of one or more of the figures in this paper are available online at http://ieeexplore.ieee.org.

Digital Object Identifier 10.1109/TSTE.2014.2305433

The VRB seems to be an excellent candidate for large-scale PV applications, although it is not price-competitive at the moment. The VRB features long service life, which means its chemical aging process is relatively slow in comparison with alternative battery technologies [11], [12]. Most importantly, the power and energy ratings of VRB are independent of each other, which increase the scalability of the VRB for PV systems of different power ratings. However, one major drawback of the VRB is the complicated electrolyte circulation system, which leads to low efficiency when the VRB is operated at less than 20% of its rated power [13].

Compared with the single-technology ESS, a hybrid ESS (HESS) can combine the advantages of each technology used, thus being more suitable for large-scale renewable energy systems. Typical combinations may include battery and supercapacitors (SCs), compressed air and SCs, battery and superconducting magnetics, and others [1].

The main challenge of using HESSs is the power sharing between different technologies [14]–[27]. The traditional concept of the power sharing is based on the response times of each technology: the high-frequency power oscillations are assigned to the short-term storage device and the low-frequency oscillations are handled by the long-term storage device [18]. A linear filter has been applied to allocate the power between a high power density device and a high energy density device in a wind farm application in [19] and [25]. A multilevel control structure, including a linear filter and an optimized controller, has been proposed recently [14], [16], [17]. The fuzzy controller has been added to a linear filter to manage a superconducting magnetic energy storage and battery HESS in [14]. Other two rule-based approaches have been introduced to adjust the power reference of an HESS based on VRB and SC in [16] and [17]. By extending this traditional concept, more optimal control techniques have been recently applied to coordinate the power of the HESS, such as sliding mode control in [20] and [22] and model predictive control in [21] and [27].

Most of the technical literature discusses the control performance of HESSs under the assumption that high power density devices such as SC can be easily scaled at high power ratings. However, the SCs have a higher power density when compared to batteries, but it is difficult to expand their power rating beyond MW level due to cell voltage unbalancing issues [28].

In this paper, an HESS based on the VRB and the SC technologies has been proposed to smooth the oscillating output power of a 1-MW grid-connected PV system in accordance with the Australian rules for semischeduled generation [29]. The proposed power management (PM) of the PV power plant is a rule-based algorithm, which consists of two stages: an

incremental power sharing scheme between the VRB and SC bank (SCB) and the rules managing the operation modes of the PV power plant. The main advantages of the proposed PM with respect to conventional techniques are as follows: reducing the required power rating of the SCB to only one-fifth of the VRB rating and avoiding the operation of the VRB at low power levels, thus increasing its overall efficiency.

The rest of this paper is organized as follows. Section II presents the simplified electrical model of the PV power plant including the HESS and its associated control strategy. In Section III, the proposed PM algorithm is introduced and all operating modes are explained in detail. The simulation results of two different case studies are presented in Section IV. Finally, Section V summarizes this work and draws the conclusion.

II. System Description and Modeling

The configuration of the proposed PV power plant including the HESS is shown in Fig. 1. All PV arrays and the energy storage units are connected to a common dc bus through dc–dc converters. The common dc bus is connected to the grid through an inverter.

A. PV System Modeling

This paper focuses on the PM of the PV power plant from a system point of view. Therefore, for simplicity purposes, a megawatt PV system can be modeled as a first-order transfer function $H_{\mathrm{PV}}(s)$ [30], as given in

$$H_{\mathrm{PV}}(s) = \frac{P_{\mathrm{nom}}}{(\sqrt{S}/(2\cdot\pi\cdot a))\cdot s + 1} \tag{1}$$

where P_{nom} is the nominal power of the PV system, S is the land area of the PV system in hectares, and a is a constant given by curve fitting in [30]. The peak power of the PV system is described as

$$\hat{P}_{\mathrm{PV}} = G \cdot H_{\mathrm{PV}}(s) \tag{2}$$

where G is the solar irradiation measured in the center of the PV system area.

B. Energy Storage Modeling

This paper focuses on the electrical performance of two different energy storage units, namely the VRB and the SCB. The detailed equivalent electrical models of VRB and SCB have been implemented to constitute the HESS.

1) VRB Modeling: The equivalent electrical model of VRB is illustrated in Fig. 2(a), which fits the experimental data very well in the steady-state analysis [31]–[33]. The stack voltage (V_{stack}) is calculated by the Nernst equation [34], as given in

$$V_{\mathrm{stack}} = m \cdot \left(V_{\mathrm{eq}} + c \cdot \ln \frac{\mathrm{SOC}}{1-\mathrm{SOC}} \right) \tag{3}$$

where m is the number of cells in the stack, V_{eq} is the single-cell voltage at 50% state of charge (SOC) and zero current, and c is a

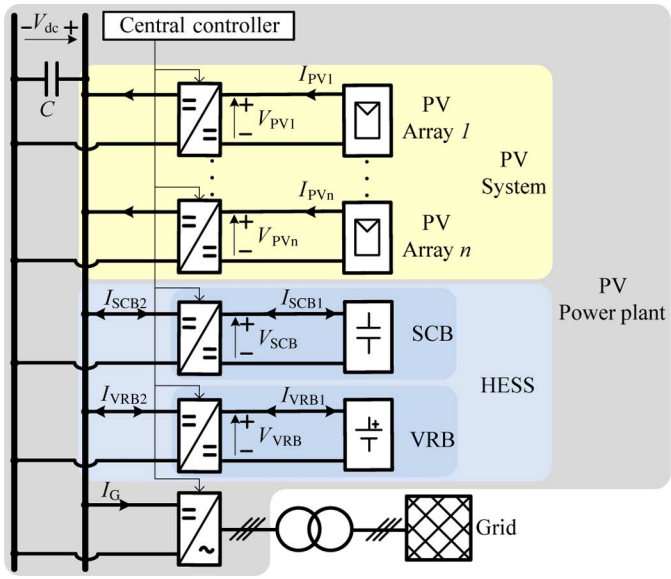

Fig. 1. Configuration of the PV power plant including the HESS.

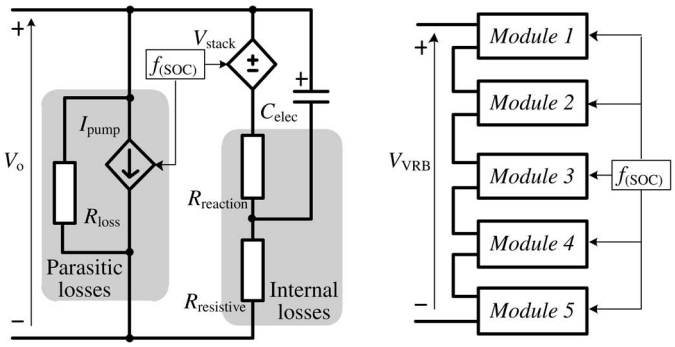

Fig. 2. Model of the VRB: (a) model of single VRB module and (b) VRB-ESS model including five modules.

constant related to the ambient temperature. The SOC of the VRB is calculated by

$$\mathrm{SOC}(k) = \mathrm{SOC}(k-1) + \frac{I_{\mathrm{stack}} \cdot V_{\mathrm{stack}} \cdot T_s}{E_{\mathrm{rating}}} \tag{4}$$

where I_{stack} is the current through the stack, T_{s} is the time step, and E_{rating} is the energy capacity of VRB.

In Fig. 2(a), the resistances R_{reaction} and $R_{\mathrm{resistive}}$ compose the internal losses of the stack, and the parasitic losses are affected by the resistance R_{loss} and a controlled current source I_{pump}. The current I_{pump} reflects the pump current required for circulating the electrolytes, which is related to the SOC.

The efficiency of the VRB power stack is inversely proportional to its operating power. Additionally, the parasitic losses significantly lower the overall efficiency of the VRB system, regardless of its operating power [13]. A power versus efficiency characteristic of the VRB model is shown in Fig. 3.

In order to expand the power rating of the VRB, numerous modules can be connected in series and/or in parallel. In this paper, the VRB energy storage unit consists of five modules connected in series, which share the same set of functions $f_{(\mathrm{SOC})}$,

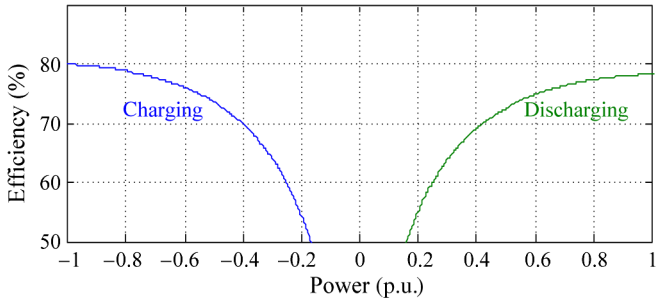

Fig. 3. Efficiency–power curve of VRB at constant 50% SOC.

TABLE I
PARAMETERS OF VRB AND SC MODELS

VRB stack parameters		Single SC parameters	
m	100	$C1$	31.7 F
V_{eq}	1.4 V	$C2$	53.2 F
c	0.0517	$C3$	20.9 F
$R_{reaction}$	0.024 Ω	$R1$	0.0296 Ω
$R_{resistive}$	0.016 Ω	$R2$	0.00494 Ω
R_{loss}	5 Ω	$R3$	0.00979 Ω
C_{elec}	0.06 F		
VRB parameters		**SC bank parameters**	
P_{rating}	250 kW	P_{rating}	50 kW
E_{rating}	20.8 kWh	E_{rating}	4.2 kWh
Low SOC	10%	Low SOC	10%
High SOC	90%	High SOC	90%
Number of stacks	5	Number in series/parallel	200/206

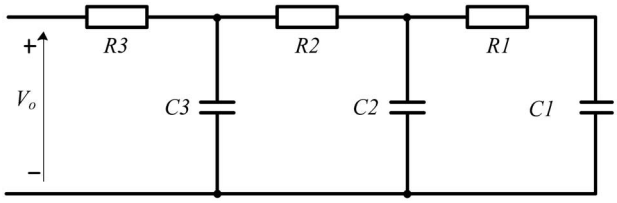

Fig. 4. Third-order Ladder SC model.

as shown in Fig. 2(b). All of the VRB model parameters are listed in Table I.

2) SCB Modeling: One of the widely used equivalent SC models is the Ladder model [35], [36]. According to a comparison study in [36], a third-order model presents excellent characteristics for a simulation time step in the order of milliseconds, which is suitable for simulating the entire PV power plant, and thus it has been considered in this paper, as shown in Fig. 4.

In order to achieve the required power and energy rating, 200 SCs are connected in series as one branch, and 206 branches are connected in parallel constituting the SCB. The parameters of the single SC and SCB are listed in Table I.

Unlike the VRB, an SC can provide high efficiency ($> 95\%$) operation across its entire power range, thus complementing well the functionality of the VRB. However, the losses caused by the voltage balancing auxiliary circuits can be quite high according to [28]. 10% auxiliary losses have been assumed for this paper.

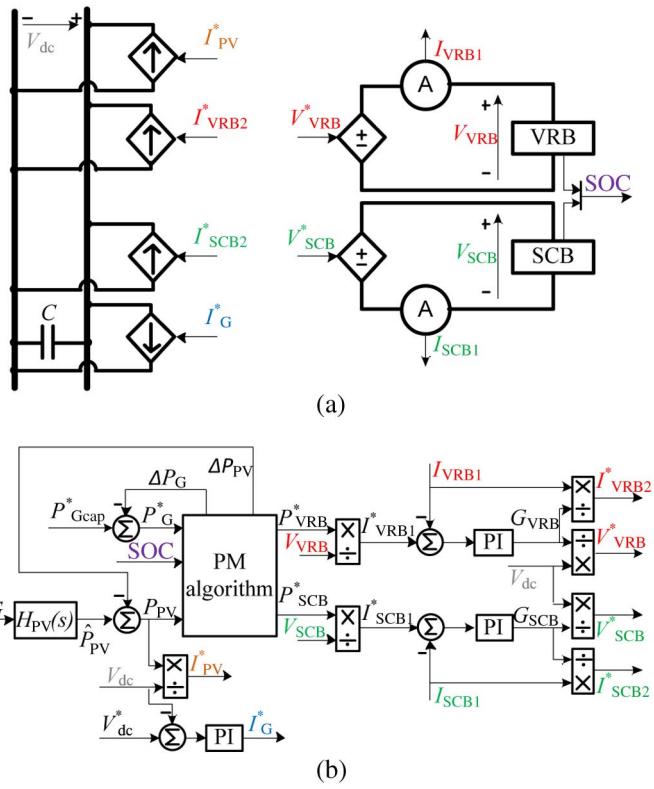

Fig. 5. Simplified model of PV plant: (a) power converters using average model and (b) control strategy of PV power plant.

C. Converters Modeling

The average models of the power converters, as shown in Fig. 5(a), are used in this paper to analyze the performance of the PV power plant in the order of hours and/or days.

All the dc–dc converters connecting the PV arrays to the common dc bus in Fig. 1 are simplified to a controlled current source (I^*_{PV}). This current source represents the entire PV system generating the power as given in (2), which is managed by the HESS and then delivered to the electricity grid by an inverter represented by a controlled current source (I^*_G).

The dc–dc converters connecting the VRB and SCB with the common dc bus are represented by two controlled current sources (I^*_{VRB2} and I^*_{SCB2}) and two controlled voltage source (V^*_{VRB} and V^*_{SCB}). Four control signals for these dc–dc converters are calculated by

$$\begin{aligned} V^*_{VRB} &= G_{VRB} \cdot V_{dc} \text{ and } I^*_{VRB2} = I_{VRB1}/G_{VRB} \\ V^*_{SCB} &= G_{SCB} \cdot V_{dc} \text{ and } I^*_{SCB2} = I_{SCB1}/G_{SCB} \end{aligned} \quad (5)$$

where V_{dc} is the voltage of the dc bus, I_{VRB1} and I_{SCB1} are the output currents of the VRB and SCB, respectively, and G_{VRB} and G_{SCB} are the gains of the VRB and SCB dc–dc converters, respectively.

D. Control Strategy of the PV Power Plant

The proposed control strategy of the PV power plant is illustrated in Fig. 5(b). This control diagram includes three inputs: G, P^*_{Gcap} and V^*_{dc}, where P^*_{Gcap} is the demand power reference, which is issued by the grid operator for every 5 min in

accordance with the Australian rules for semischeduled generation [29] and $V^*_{\rm dc}$ is the reference of the dc bus voltage. There are six output signals including four current references ($I^*_{\rm PV}$, $I^*_{\rm G}$, $I^*_{\rm VRB2}$, and $I^*_{\rm SCB2}$) and two voltage references ($V^*_{\rm VRB}$ and $V^*_{\rm SCB}$), which constitute all control signals for the dc–dc converters shown in Fig. 1.

The reference $I^*_{\rm PV}$ is generated from dividing the PV output power by the dc bus voltage. A PI controller regulates the voltage of the dc bus through the grid current reference $I^*_{\rm G}$. The power references of VRB and SCB ($P^*_{\rm VRB}$ and $P^*_{\rm SCB}$) are given by the proposed PM algorithm, which regulates the gains of the dc–dc converters ($G_{\rm VRB}$ and $G_{\rm SCB}$) by two PI controllers. According to (5), these gains generate the last four control references. Eventually, the operating points of the VRB and the SCB are regulated, thus delivering and/or absorbing power to/from the common dc bus.

The output power of the PV power plant should not exceed the demand power reference ($P^*_{\rm Gcap}$) according to the Australian rules for semischeduled generation [29]. Based on economic considerations, the output power of the PV plant should always be maximized. Therefore, the HESS is used to smooth the intermittent power ($P_{\rm PV}$) and to maintain the output power as close to $P^*_{\rm Gcap}$ as possible. Specifically, the HESS is required to store the excess power, when $\hat{P}_{\rm PV}$ is higher than $P^*_{\rm Gcap}$. On the contrary, the HESS compensates the power gap, when $\hat{P}_{\rm PV}$ is lower than $P^*_{\rm Gcap}$.

Under some circumstances, the HESS is limited by its rating constraints and cannot deliver enough power to compensate the deficit of the PV output power. In this case, the power delivered to the grid has to be reduced by $\Delta P_{\rm G}$. The reference of power delivered to the grid ($P^*_{\rm G}$) is introduced in (6). On the contrary, the PV output power might be in excess; therefore, the PV output power is curtailed by $\Delta P_{\rm PV}$, which is presented in (7). Finally, the power reference of the HESS is calculated as (8), which is shared between the VRB and the SCB by the proposed PM algorithm, as follows:

$$P^*_{\rm G} = P^*_{\rm Gcap} - \Delta P_{\rm G} \tag{6}$$

$$P_{\rm PV} = \hat{P}_{\rm PV} - \Delta P_{\rm PV} \tag{7}$$

$$P^*_{\rm HESS} = P_{\rm PV} - P^*_{\rm G}. \tag{8}$$

The PM algorithm is detailed in Section III.

III. PM Algorithm

The proposed PM algorithm of the PV power plant is a heuristic rule-based algorithm. The heuristic control rules are developed based on the Australian rules for semischeduled generation [29] and the rating constraints of VRB and SCB. Specifically, the Australian grid code requires the PV power plant to generate a constant power below $P^*_{\rm Gcap}$ in every 5 min dispatch interval. Additionally, the rating constraints of VRB and SCB are described in (9)

$$\begin{aligned} &0.05\ \text{p.u.} \le |P_{\rm VRB}| \le 0.25\ \text{p.u.} \\ &|P_{\rm SCB}| \le 0.05\ \text{p.u.} \\ &L_{\rm VRB} \le {\rm SOC}_{\rm VRB} \le H_{\rm VRB} \\ &L_{\rm SCB} \le {\rm SOC}_{\rm SCB} \le H_{\rm SCB} \end{aligned} \tag{9}$$

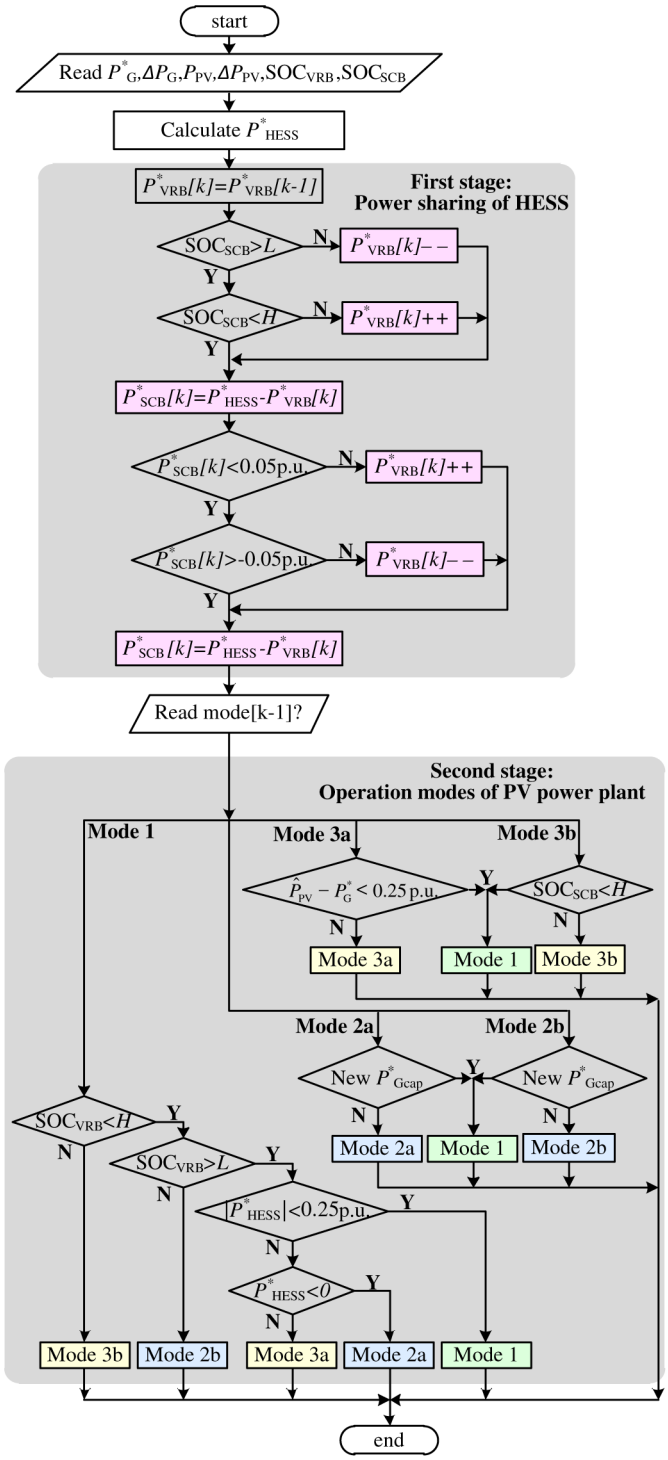

Fig. 6. Flowchart of the proposed PM algorithm.

where the power limits have been normalized to per unit (p.u.) by the rated power of the PV power plant and $L_{\rm VRB}/H_{\rm VRB}$ and $L_{\rm SCB}/H_{\rm SCB}$ represent the low/high SOC limit of VRB and SCB, respectively.

The flowchart of the proposed PM algorithm is detailed in Fig. 6. The first stage of the algorithm consists of an incremental power sharing scheme, which gives the power references to the VRB and SCB. The second stage of the algorithm decides the operation modes of the PV power plant, which indirectly affects

the power references of the HESS by changing P_G^* and P_{PV} in the feedback loop as shown in Fig. 5.

A. First Stage: Power Sharing of HESS

The first stage of the PM algorithm handles the power sharing between the VRB and the SCB. The power reference P_{HESS}^* is divided into two parts: P_{VRB}^* and P_{SCB}^*. In order to reduce the operating points of VRB, the reference P_{VRB}^* is regulated to several incremental steps. The P_{VRB}^* value is kept constant until the difference between P_{HESS}^* and P_{VRB}^* is higher than one incremental step, as shown in Fig. 7. Furthermore, while P_{VRB}^* is kept constant, the SCB handles the oscillating part of P_{HESS}^*, as in

$$P_{SCB}^* = P_{HESS}^* - P_{VRB}^*. \tag{10}$$

As a consequence, the minimum power rating of the SCB has to be equal to one incremental step.

As mentioned in Section II, the efficiency of VRB drops significantly at low power operating points. In this paper, the critical low power of the VRB is chosen to be 0.05 p.u. as given in (9), which ensures the efficiency over 50%. In order to avoid the VRB operating below the critical low power, the minimum incremental step is 0.05 p.u. For simplicity purposes, the power rating of the SCB is chosen at 0.05 p.u. as shown in Table I.

The SOC constraints of SCB are also considered by the power sharing scheme. If SOC_{SCB} reaches its lower or higher limits, decreasing or increasing P_{VRB}^* by one increment (0.05 p.u.) reverses the operating mode of SCB from discharging to charging and vice versa, thus bringing the SOC_{SCB} within its limits, as shown in Fig. 6.

B. Second Stage: Operation Modes of PV Power Plant

The second stage of the PM algorithm decides the operation modes of the PV power plant, as shown in Fig. 6. These operation modes are based on the following constraints: VRB power rating, SOC of the VRB, and the Australian grid code requirements. Specifically, the operation modes are classified into three main categories: normal power mode, deficit power mode, and excess power mode, as shown in Table II. Additionally, there are two different subcategories in deficit power mode and excess power mode, respectively. The operation modes of the PV power plant and their ranges are illustrated in Fig. 8.

1) Normal Power Mode: The normal power mode is called Mode 1, which is presented in green color. In this mode, the SOC of the VRB satisfies the constraints given in (9), and the power reference of HESS given in (8) is also within the limit, as shown in Fig. 8. Therefore, both ΔP_{PV} and ΔP_G are equal to zero, as shown in Table II. Also, the power references of VRB and SCB are given by the power sharing scheme of HESS.

2) Deficit Power Mode: The deficit power mode has two subcategories called Mode 2a and Mode 2b, which are presented in blue color. In these modes, the demand power reference P_{Gcap}^* is reduced by ΔP_G, thus resulting P_G^* as shown in Fig. 5. This is due to the fact that the output power of PV plant is in deficit and it is not able to maintain the power delivered to the grid at the required value by P_{Gcap}^*.

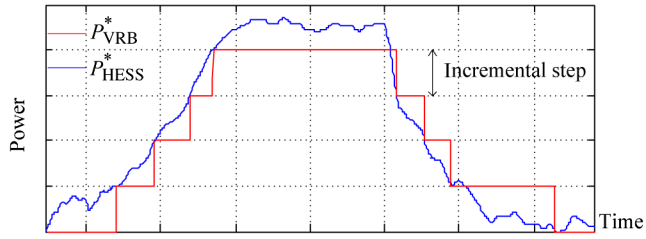

Fig. 7. Incremental operation of the VRB power reference.

TABLE II
OPERATION MODES AND ACTIONS

Categories	Modes	ΔP_G	ΔP_{PV}	P_{VRB}^*	P_{SCB}^*
Normal power mode	1	0	0	$P_{VRB}^*[k]$	$P_{SCB}^*[k]$
Deficit power mode	2a	0.05 p.u.	0	$P_{VRB}^*[k]$	$P_{SCB}^*[k]$
	2b	0.35 p.u.	0		
Excess power mode	3a	0	$\hat{P}_{PV} - P_G^* - 0.25$ p.u.	$P_{VRB}^*[k]$	$P_{SCB}^*[k]$
	3b	0	$\hat{P}_{PV} - P_G^*$	0	0

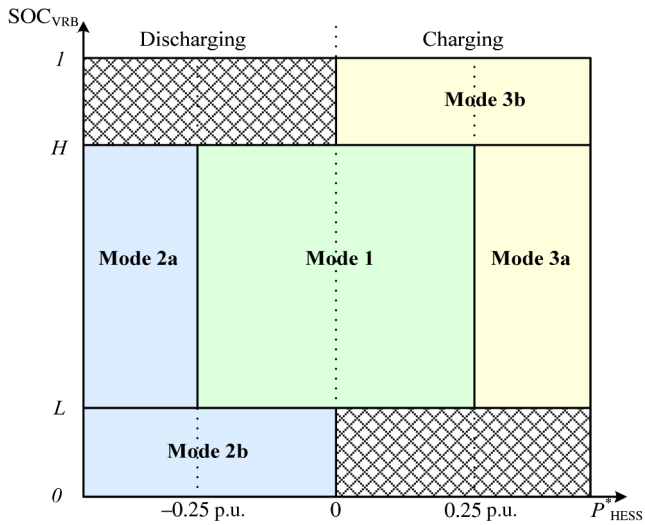

Fig. 8. Operation modes of PV power plant and their ranges.

The only difference between Mode 2a and Mode 2b is the value of ΔP_G, the rest of actions remaining the same, as shown in Table II.

If the PV plant exits Mode 1 by exceeding the negative limit of P_{HESS}^*, then Mode 2a is activated. A small value is chosen for ΔP_G in Mode 2a, as the SOC of VRB is within the range and thus the VRB can continue to discharge. On the contrary, if the SOC of the VRB reaches its lower limit, then Mode 2b is activated. In this mode, a higher value of ΔP_G is chosen, as shown in Table II. This ensures that the operating point of the VRB is reversed from discharging to charging.

If the PV plant already operates in one of the deficit power modes (Mode 2a or Mode 2b), then the mode is maintained until a new P_{Gcap}^* is released by the grid operator, thus minimizing any possible penalties [29]. The new P_{Gcap}^* reflects the next 5-min dispatch interval.

3) Excess Power Mode: The excess power mode also has two subcategories called Mode 3a and Mode 3b, which are presented in yellow color. In these modes, the PV system generates significantly more power than P^*_{Gcap}. At the same time, the HESS cannot handle all the excess power due to its rating limits. Therefore, the output power of PV system has to be curtailed by ΔP_{PV} in order to fulfill the grid code requirements [29].

If the PV plant exits Mode 1 by exceeding the positive limit of P^*_{HESS}, then Mode 3a is activated. In this mode, the PV system only curtails the amount of power that exceeds the power rating of VRB, as the SOC of VRB is within the range, thus the VRB can continue to charge. In this mode, the power references of VRB and SCB are given by the power sharing scheme of HESS. On the contrary, if the SOC of VRB reaches its upper limit, then Mode 3b is activated. In this mode, the PV system curtails the amount of power exceeding P^*_{Gcap}. In Mode 3b, the power references of VRB and SCB are set to zero, as shown in Table II.

If the PV plant already operates in Mode 3a, then this mode is maintained until the amount of power exceeding P^*_{Gcap} is within the range of the VRB-rated power. If the PV plant already operates in Mode 3b, then this mode is maintained until the SOC of the VRB returns below its upper limit.

IV. Simulation Results

A 1-MW PV power plant, as presented in Fig. 1, has been implemented in MATLAB/Simulink and PLECS software platform. Typically, the area of such PV plant is approximated to 4 ha. The PV simulation model uses the real solar irradiation data measured at St. Lucia campus of the University of Queensland, Brisbane, Australia [37]. The common dc bus has been regulated to a constant voltage of 1000 V. As discussed in Section II, all power converters have been simulated as average models in order to run a simulation of the entire PV power plant in the time frame of hours and/or days. The HESS combining a 250-kW VRB and a 50-kW SCB has been investigated under two different scenarios: half-hour operation and one-week operation. All power values presented in this section are normalized to per unit (p.u.) by 1 MW.

A. Half-Hour Operation

A 30-min window of solar irradiation data has been carefully selected in order to trigger all the operation modes with a good resolution. Additionally, the SOC of HESS has particularly initialized at 0.8 p.u. for the VRB and 0.6 p.u. for the SCB. Moreover, the profile of P^*_{Gcap} has also been chosen carefully in order to trigger all the operation modes within half an hour. The simulation results of this case are presented in Fig. 9. The PV plant mainly operates in Mode 1, as it can be noticed from Fig. 9(e) and (f).

By triggering all the operation modes, the proposed PM algorithm successfully ensures that the VRB and SCB operate within their rating constraints in terms of power and SOC, as shown in Fig. 9(b)–(d). Additionally, the VRB only operates at incremental power levels as discussed in Section III-A. Therefore, the VRB only operates above the critical low power of 0.05 p.u., thus improving its efficiency.

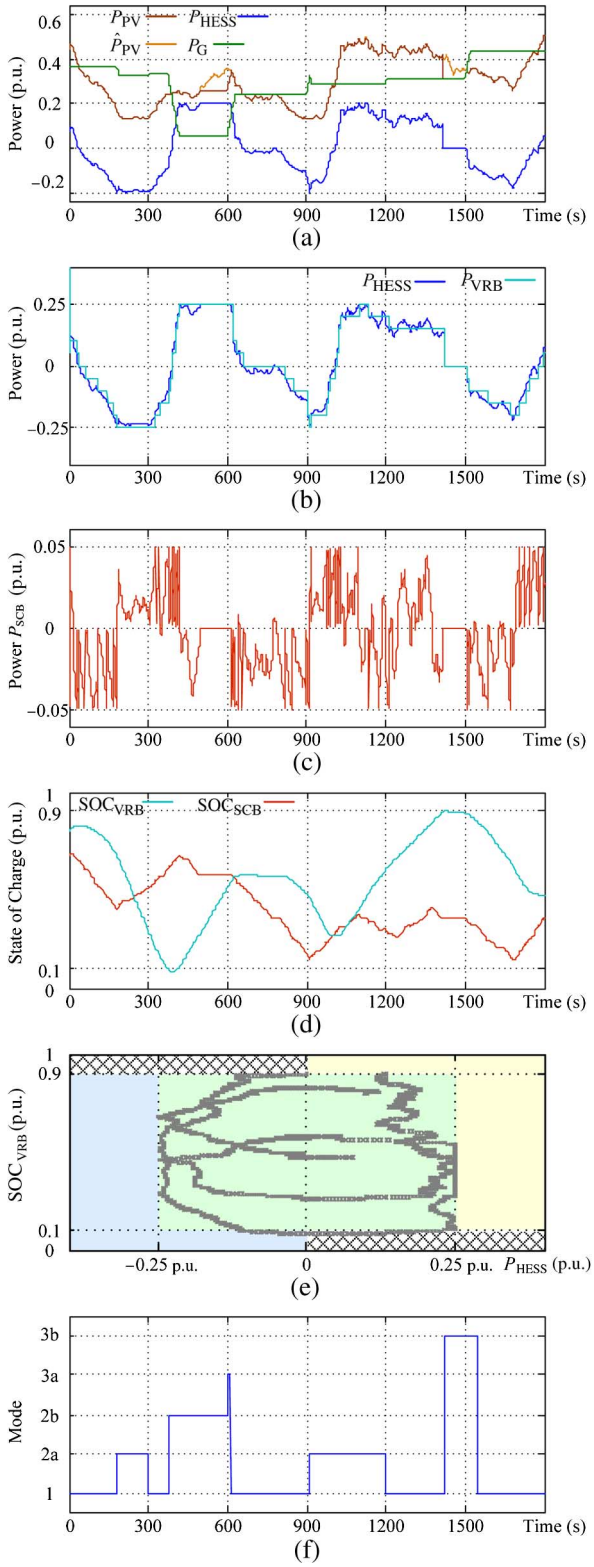

Fig. 9. Simulation results of half-hour operation: (a)–(c) power profile of PV plant; (d) SOC of HESS; (e) operating points of PV plant; and (f) operation modes in time series.

The power delivered to the grid is maintained constant in most of 5-min dispatch intervals, as it can be seen in Fig. 9(a). Only three alterations in the dispatch intervals occur around 200s, 400s, and 900s, respectively. These alterations were caused by the operation in deficit power modes.

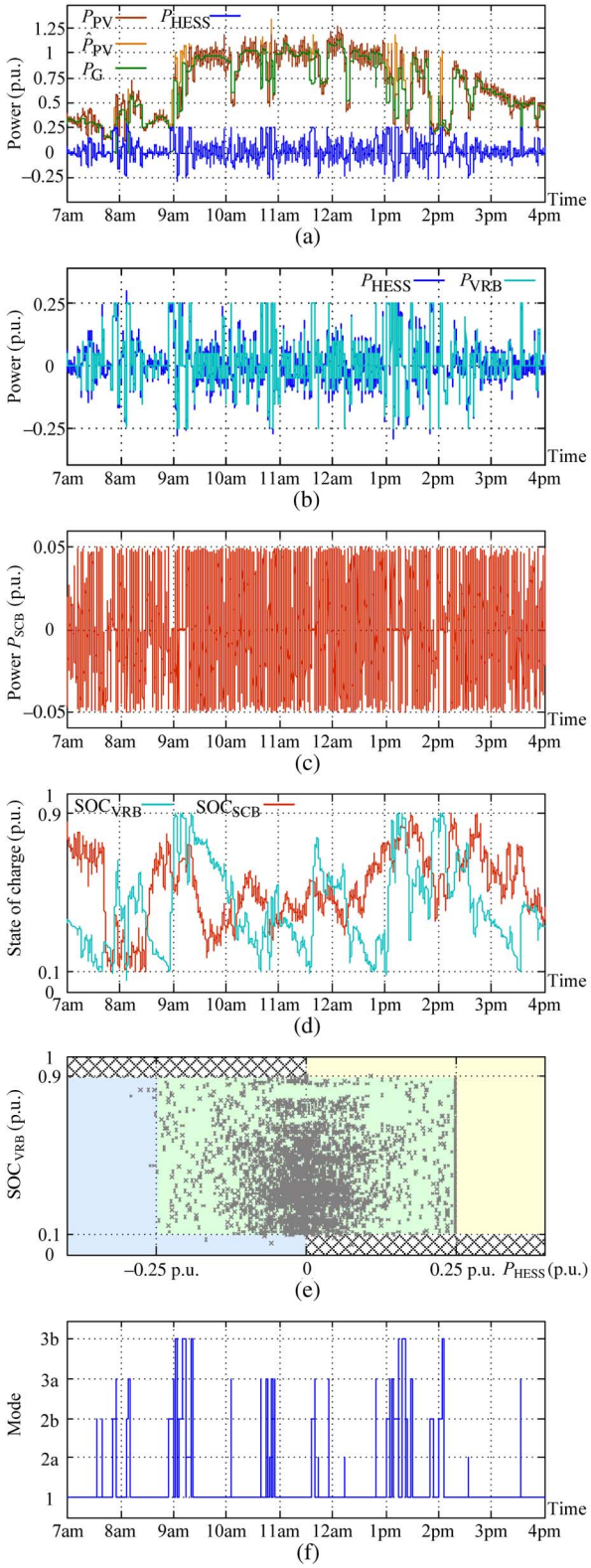

Fig. 10. Simulation results of one day operation on November 12, 2013: (a)–(c) power profile of PV plant; (d) SOC of HESS; (e) operating points of PV plant; and (f) operation modes in time series.

B. One-Week Operation

A one-week operation has been considered in this case study in order to verify the reliability of the proposed algorithm. The solar irradiation data of 1 week chosen for this case is based on the worst case scenario for 2013 at St. Lucia campus. For simplicity purposes, the SOC of both VRB and SCB have been reset to 0.5 p. u. at end of each day, so that the simulation of each day can be performed independently. Moreover, P^*_{Gcap} is chosen as the average value of the PV output power for every dispatch interval. The results of one-day operation on November 12, 2013 are presented in Fig. 10, and Fig. 11 shows the results of a full week operation. As it can be seen from Fig. 10(e) and (f), the PV plant mainly operates in Mode 1. Similarly to the half-hour operation, the power delivered to grid is maintained constant in most of dispatch intervals, as shown in Fig. 10(a). As it can be observed from Fig. 11(b) and (c), the PV output power has been significantly smoothed by the proposed PM algorithm. Additionally, even though the PV plant goes beyond the constraints occasionally, the algorithm always returns the operating points of the PV plant within the constraints, as shown in Fig. 11(d). It is worth noticing that the operating points beyond the constraints are in the particular areas, such as below the negative power limit of P^*_{HESS} and below the lower limit of $\mathrm{SOC}_{\mathrm{VRB}}$. This is due to the fact that P^*_{G} has a maximum rate of ramping up/down according to the grid code requirements [29].

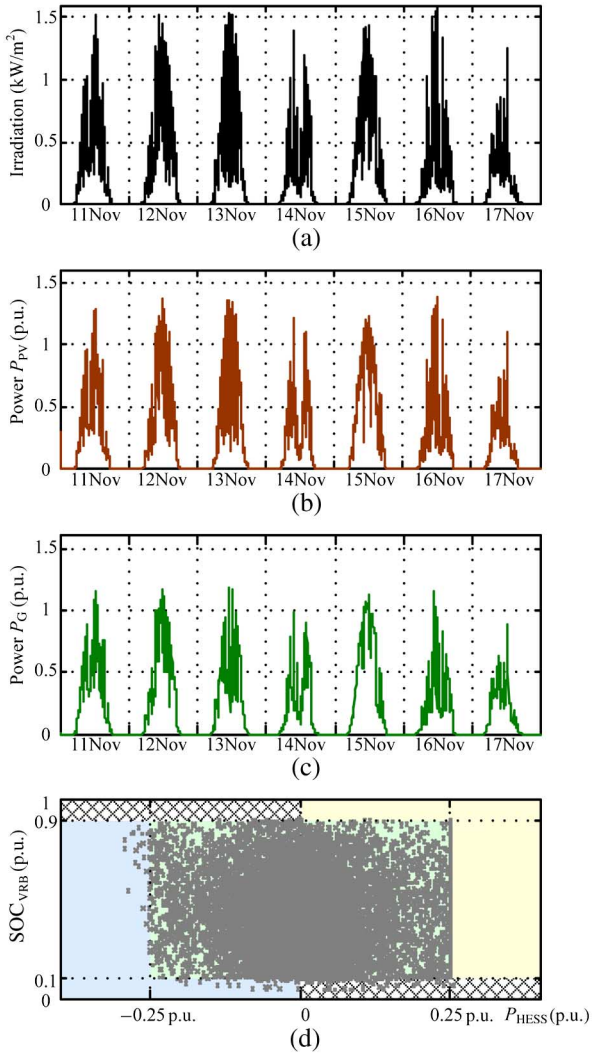

Fig. 11. Simulation results of full week operation from November 11, 2013 to November 17, 2013: (a) solar irradiation profile; (b) profile of PV output power; (c) profile of power delivered to grid; and (d) operating points of PV plant.

V. Conclusion

This paper has presented an HESS combining the VRB and SCB for smoothing the output power of a 1-MW grid-connected PV power plant. According to the Australian rules for semi-scheduled generation [29], the output power of the PV plant is maintained to a fixed cap for every 5 min.

A rule-based PM has been proposed and investigated under two different scenarios: half-hour operation and one-week operation. It has been proven that the proposed PM algorithm can meet the Australian grid codes requirements. Furthermore, the required power rating of the SCB has been reduced to only one-fifth of the VRB rating. Additionally, the operation of the VRB at low power levels has been avoided, thus increasing its overall efficiency. Additionally, the SOC of VRB and SCB were maintained within their limits at all times.

References

[1] S. Vazquez, S. M. Lukic, E. Galvan, L. G. Franquelo, and J. M. Carrasco, "Energy storage systems for transport and grid applications," *IEEE Trans. Ind. Electron.*, vol. 57, no. 12, pp. 3881–3895, Dec. 2010.

[2] M. H. Nehrir, C. Wang, K. Strunz, H. Aki, R. Ramakumar, J. Bing *et al.*, "A review of hybrid renewable/alternative energy systems for electric power generation: Configurations, control, and applications," *IEEE Trans. Sustain. Energy*, vol. 2, no. 4, pp. 392–403, Oct. 2011.

[3] J. M. Carrasco, L. G. Franquelo, J. T. Bialasiewicz, E. Galvan, R. C. P. Guisado, M. A. M. Prats *et al.*, "Power-electronic systems for the grid integration of renewable energy sources: A survey," *IEEE Trans. Ind. Electron.*, vol. 53, no. 4, pp. 1002–1016, Jun. 2006.

[4] M. Bragard, N. Soltau, S. Thomas, and R. W. De Doncker, "The balance of renewable sources and user demands in grids: Power electronics for modular battery energy storage systems," *IEEE Trans. Power Electron.*, vol. 25, no. 12, pp. 3049–3056, Dec. 2010.

[5] S. Teleke, M. E. Baran, S. Bhattacharya, and A. Q. Huang, "Rule-based control of battery energy storage for dispatching intermittent renewable sources," *IEEE Trans. Sustain. Energy*, vol. 1, no. 3, pp. 117–124, Oct. 2010.

[6] Y. Riffonneau, S. Bacha, F. Barruel, and S. Ploix, "Optimal power flow management for grid connected PV systems with batteries," *IEEE Trans. Sustain. Energy*, vol. 2, no. 3, pp. 309–320, Jul. 2011.

[7] G. Wang, M. Ciobotaru, and V. G. Agelidis, "Minimising output power fluctuation of large photovoltaic plant using vanadium redox battery storage," in *Proc. 6th IET PEMD.* Bristol, U.K., 2012, pp. D41–D41.

[8] S. C. Smith, P. K. Sen, and B. Kroposki, "Advancement of energy storage devices and applications in electrical power system," in *Proc. Power Energy Soc. Gen. Meeting,* 2008, pp. 1–8.

[9] H. Chen, T. N. Cong, W. Yang, C. Tan, Y. Li, and Y. Ding, "Progress in electrical energy storage system: A critical review," *Progress Nat. Sci.*, vol. 19, pp. 291–312, Oct. 3, 2009.

[10] A. M. Gee, F. V. P. Robinson, and R. W. Dunn, "Analysis of battery lifetime extension in a small-scale wind-energy system using supercapacitors," *IEEE Trans. Energy Convers.*, vol. 28, no. 1, pp. 24–33, Mar. 2013.

[11] M. Skyllas-Kazacos, G. Kazacos, G. Poon, and H. Verseema, "Recent advances with UNSW vanadium-based redox flow batteries," *Int. J. Energy Res.*, vol. 34, pp. 182–189, 2010.

[12] M. Skyllas-Kazacos, M. Chakrabarti, S. Hajimolana, F. Mjalli, and M. Saleem, "Progress in flow battery research and development," *J. Electrochem. Soc.*, vol. 158, pp. R55–R79, 2011.

[13] H. Bindner, C. Ekman, O. Gehrke, and F. Isleifsson, "Characterization of vanadium flow battery, revised," Tech. Rep. Riso-R-1753(EN), 2011.

[14] T. Ise, M. Kita, and A. Taguchi, "A hybrid energy storage with a SMES and secondary battery," *IEEE Trans. Appl. Supercond.*, vol. 15, no. 2, pp. 1915–1918, Jun. 2005.

[15] S. Lemofouet and A. Rufer, "A hybrid energy storage system based on compressed air and supercapacitors with maximum efficiency point tracking (MEPT)," *IEEE Trans. Ind. Electron.*, vol. 53, no. 4, pp. 1105–1115, Jun. 2006.

[16] C. Abbey, K. Strunz, and G. Joos, "A knowledge-based approach for control of two-level energy storage for wind energy systems," *IEEE Trans. Energy Convers.*, vol. 24, no. 2, pp. 539–547, Jun. 2009.

[17] C. Abbey, L. Wei, and G. Joos, "An online control algorithm for application of a hybrid ESS to a wind-diesel system," *IEEE Trans. Ind. Electron.*, vol. 57, no. 12, pp. 3896–3904, Dec. 2010.

[18] A. Etxeberria, I. Vechiu, H. Camblong, and J. M. Vinassa, "Hybrid energy storage systems for renewable energy sources integration in microgrids: A review," in *Proc. IPEC,* 2010, pp. 532–537.

[19] L. Wei, G. Joos, and J. Belanger, "Real-time simulation of a wind turbine generator coupled with a battery supercapacitor energy storage system," *IEEE Trans. Ind. Electron.*, vol. 57, no. 4, pp. 1137–1145, Apr. 2010.

[20] A. Etxeberria, I. Vechiu, H. Camblong, and J. M. Vinassa, "Comparison of sliding mode and PI control of a hybrid energy storage system in a microgrid application," *Energy Procedia*, vol. 12, pp. 966–974, 2011.

[21] X. Han, F. Chen, X. Cui, Y. Li, and X. Li, "A power smoothing control strategy and optimized allocation of battery capacity based on hybrid storage energy technology," *Energies*, vol. 5, pp. 1593–1612, 2012.

[22] F. Liu, J. Liu, B. Zhang, H. Zhang, and U. Hasan Saad, "Energy management of hybrid energy storage system (HESS) based on sliding mode control," in *Proc. 7th IPEMC,* 2012, pp. 406–410.

[23] C. Mid-Eum, K. Seong-Woo, and S. Seung-Woo, "Energy management optimization in a battery/supercapacitor hybrid energy storage system," *IEEE Trans. Smart Grid*, vol. 3, no. 1, pp. 463–472, Mar. 2012.

[24] G. Wang, M. Ciobotaru, and V. G. Agelidis, "PV power plant using hybrid energy storage system with improved efficiency," in *Proc. 3rd IEEE PEDG.* Aalborg, Denmark, 2012, pp. 808–813.

[25] J. W. Shim, Y. Cho, S. J. Kim, S. W. Min, and K. Hur, "Synergistic control of SMES and battery energy storage for enabling dispatchability of renewable energy sources," *IEEE Trans. Appl. Supercond.*, vol. 23, no. 3, pp. 5701205–5701205, Jun. 2013.

[26] Z. Yixin, Z. Fang, and S. Hongtao, "Power management strategy research for a photovoltaic-hybrid energy storage system," in *Proc. IEEE ECCE Asia,* 2013, pp. 842–848.

[27] B. Hredzak, V. G. Agelidis, and J. Minsoo, "A model predictive control system for a hybrid battery-ultracapacitor power source," *IEEE Trans. Power Electron.*, vol. 29, no. 3, pp. 1469–1479, Mar. 2014.

[28] P. Sharma and T. S. Bhatti, "A review on electrochemical double-layer capacitors," *Energy Convers. Manage.*, vol. 51, pp. 2901–2912, 2010.

[29] AEMC (May 2013). *National Electricity Rules Version 55* [Online]. Available: http://www.aemc.gov.au/Electricity/National-Electricity-Rules/Current-Rules.html.

[30] J. Marcos, L. Marroyo, E. Lorenzo, D. Alvira, and E. Izco, "From irradiance to output power fluctuations: The PV plant as a low pass filter," *Prog. Photovoltaics: Res. Appl.*, vol. 19, pp. 505–510, 2011.

[31] M. Gatrell and N. Gupta, "Developing a simple flow battery model—Initial concepts," Electricity Storage Systems Project, National Research Council Canada (NRC) document.

[32] J. Chahwan, "VRB and li-ion battery modelling and performance in wind energy applications," Master in Engineering, Depart. Electrical and Computer Engineering, McGill Univ., Montréal, Canada, 2007.

[33] J. Chahwan, C. Abbey, and G. Joos, "VRB modelling for the study of output terminal voltages, internal losses and performance," in *Proc. Elect. Power Conf.*, Canada, 2007, pp. 387–392.

[34] A. Wahl, "A short history of electrochemistry," *Galvanotechtnik*, vol. 96, pp. 1820–1828, 2005.

[35] J. R. Miller, "Battery-capacitor power source for digital communication applications: Simulations using advanced electrochemical capacitors," in *Proc. Symposia at ECS,* 1995, pp. 246–254.

[36] R. A. Dougal, L. Gao, and S. Liu, "Ultracapacitor model with automatic order selection and capacity scaling for dynamic system simulation," *J. Power Sources*, vol. 126, pp. 250–257, 2004.

[37] The University of Queensland. (2013, Mar. 25). *UQ SOLAR Photovoltaic Live Data* [Online]. Available: http://uqld.smartersoft.com.au/user/reportEnergy.php.

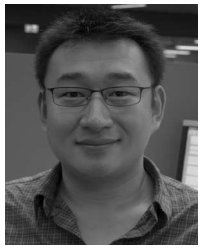

Guishi Wang (S'10) was born in Hohhot, China. He received the B.Eng. degree in electrical engineering and automation from Northwestern Polytechnic University, Xi'an, China, in 2007. He is currently working toward the Ph.D. degree in electrical engineering at the University of New South Wales, Sydney, Australia.

His research interests include the power management of hybrid energy storage system and the integration of vanadium redox battery in large-scale PV power plants.

Mihai Ciobotaru (S'04–M'08) was born in Galati, Romania. He received the B.Sc. and M.Sc. degrees in electrical engineering from University of Galati, Romania, in 2002 and 2003, respectively. In February 2009, he received the Ph.D. degree in electrical engineering from the Institute of Energy Technology, Aalborg University, Denmark.

From 2003 to 2004, he was employed as Associate Lecturer with the University of Galati. From 2007 to 2010, he was working as an Associate Research Fellow with the Institute of Energy Technology. In 2010, he joined the School of Electrical Engineering and Telecommunications, University of New South Wales (UNSW), Australia. He currently works as a Research Fellow at the Australian Energy Research Institute, UNSW. His main research activities and interests are advanced control of power converters for power flow management in electricity networks, grid voltage monitoring techniques for single-phase and three-phase voltage systems, islanding detection techniques for grid-connected PV inverters, line impedance estimation in distribution networks, and power management of battery energy storage systems.

Vassilios G. Agelidis (S'89–M'91–SM'00) was born in Serres, Greece. He received the B.Eng. degree in electrical engineering from the Democritus University of Thrace, Thrace, Greece, in 1988, the M.S. degree in applied science from Concordia University, Montreal, Quebec, Canada, in 1992, and the Ph.D. degree in electrical engineering from the Curtin University, Perth, Western Australia, Australia, in 1997.

He was with the School of Electrical and Computer Engineering, Curtin University from 1993 to 1999. In 2000, he joined the University of Glasgow, Glasgow, U.K., as a Research Manager at the Glasgow-Strathclyde Centre for Economic Renewable Power Delivery. He is currently the Director of the Australian Energy Research Institute, the University of New South Wales, Sydney, New South Wales, Australia. From January 2005 to December 2006, he was the Inaugural Chair of Power Engineering in the School of Electrical, Energy and Process Engineering, Murdoch University, Perth. From December 2006 to June 2010, he was the Energy Australia Chair of Power Engineering at the University of Sydney.

Dr. Agelidis received the Advanced Research Fellowship from the United Kingdom's Engineering and Physical Sciences Research Council in 2004. He was the Vice President Operations within the IEEE Power Electronics Society for 2006–2007. He was an Associate Editor of the IEEE POWER ELECTRONICS LETTERS from 2003 to 2005, and served as the Power Electronics Society (PELS) Chapter Development Committee Chair from 2003 to 2005. He was an AdCom Member of IEEE PELS for 2007–2009 and the Technical Chair of the 39th IEEE Annual Power Electronics Specialists Conference, Rhodes, Greece.